

# ADVANCED OPTICAL MATERIALS

## Supporting Information

for *Advanced Optical Materials*, DOI: 10.1002/adom.201400369

All-Around SiN Stressor for High and Homogeneous Tensile Strain in Germanium Microdisk Cavities

*Abdelhamid Ghrib,\* Moustafa El Kurdi,\* Mathias Prost, Sébastien Sauvage, Xavier Checoury, Grégoire Beaudoin, Marc Chaigneau, Razvigor Ossikovski, Isabelle Sagnes, and Philippe Boucaud*

## Supporting Information

for *Adv. Opt. Mater.*, DOI: 10.1002/ adom.201400369

### Modal Gain Calculation

*Abdelhamid Ghrib,\* Moustafa El Kurdi,\* Mathias Prost, Sébastien Sauvage, Xavier Checoury, Grégoire Beaudoin, Marc Chaigneau, Razvigor Ossikovski, Isabelle Sagnes, Philippe Boucaud*

The spatial distribution of strain across the germanium layer is obtained by finite element modelling (FEM) of the structure assuming a 2D axisymmetric geometry calculation similarly to Ref. [1]. The FEM analysis provides the in-plane strain distribution across the Ge layer as shown in **Figure S1** for different types of structures studied in this work.

The spatial distribution of the strain tensor elements are then introduced into the modelling of the Ge band structure in the framework of a 30 band **k.p** formalism.<sup>[2]</sup> The model allows one to calculate the dipolar matrix elements in TM and TE polarizations for the  $\Gamma$ -HH and  $\Gamma$ -LH transitions. The energies of the  $\Gamma$  and the L conduction band valleys and the dipolar matrix elements are calculated using the strain profile as obtained by the FEM analysis. **Figure S2a** shows an example of the band energies variation across the germanium layer for the all-around SiN strained structure. The tensile strain induces a splitting of the valence band, hence the direct optical transition involves both  $\Gamma$ -HH and  $\Gamma$ -LH transitions at separated energies.

The dipolar matrix elements variation across the germanium layer is calculated using the **k.p** formalism as:

$$D_{HH,LH}^{TE,TM} = \frac{m_0}{\hbar} \langle u_{\Gamma} | \vec{\varepsilon} \cdot \vec{\nabla}_k H_{k,p} | u_{HH,LH} \rangle_{k=0} \quad (S1)$$

where  $|u_{\Gamma}\rangle$  and  $|u_{HH,LH}\rangle$  are the light hole (LH), heavy hole (HH) zone centre Bloch functions and the  $\Gamma$  conduction band eigenwavevectors respectively.

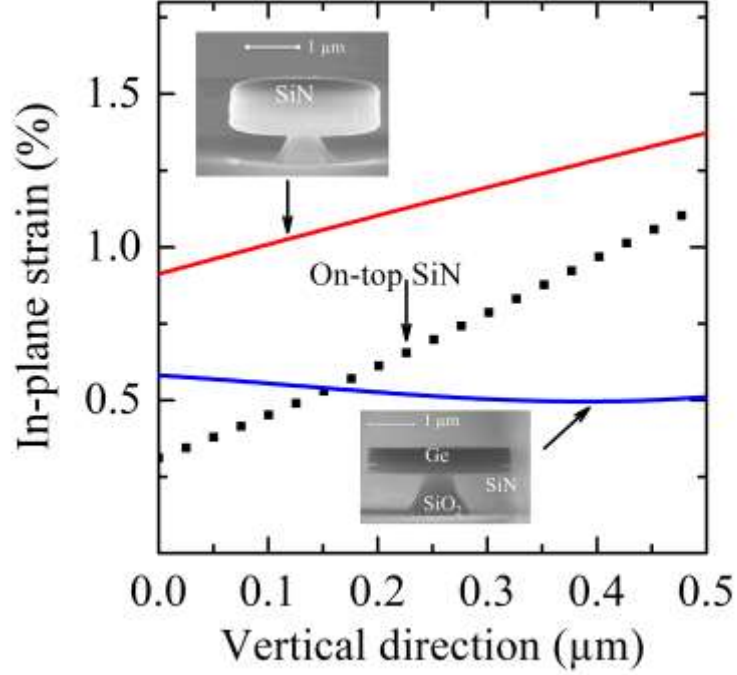


**Figure S1.** Finite element modelling of in-plane biaxial tensile strain profile across the Ge layer at the centre of a microdisk after SiO<sub>2</sub> under-etching: stressor layer at the bottom only (blue curve), stressor layer on-top only (squares) and all-around stressed microdisk (red curve).

$H_{k,p}$  is the  $\mathbf{k}\cdot\mathbf{p}$  Hamiltonian as presented in Ref. [2]. The TE and TM polarizations are defined by the orientation of the polarization vector  $\vec{\epsilon}$  of the interacting electromagnetic field. Figure S2b shows the dipolar matrix elements spatial profile calculated for both  $\Gamma$ -HH and  $\Gamma$ -LH transitions in TE and TM polarizations. The gain profile associated with each transition and polarization type across the germanium layer is then calculated using an effective-mass approach following this equation:<sup>[3]</sup>

$$\alpha_{TE,TM}^{HH,LH}(\hbar\omega) = C_0 \rho_{HH,LH}(\hbar\omega - E_{\Gamma,(HH,LH)}) |D_{HH,LH}^{TE,TM}|^2 \times [f_c(\hbar\omega - E_{\Gamma,(HH,LH)}) - f_v(\hbar\omega - E_{\Gamma,(HH,LH)})] \quad (S2)$$

Submitted to

This equation is written in a condensed form since it involves four gain formulas, *i.e.* for  $\Gamma$ -

HH and  $\Gamma$ -LH transitions and in TE and TM polarizations. In **Equation S2**  $C_0 = \frac{\pi e^2}{n_r c \epsilon_0 m_0^2 \omega}$

where  $e$  the elementary electron charge,  $n_r$  the optical refractive index of germanium,  $c$  the

light speed in vacuum,  $\epsilon_0$  the vacuum permittivity,  $m_0$  the electron mass,  $E_{\Gamma,(HH,LH)}$  are direct

band gap energies ( $E_{\Gamma} - E_{HH}$  and  $E_{\Gamma} - E_{LH}$ ),  $\hbar\omega$  the transition energy,  $f_c$  and  $f_v$  are Fermi

statistics distribution and  $\rho_{HH,LH}(\hbar\omega - E_{\Gamma,(HH,LH)}) = \frac{1}{2\pi^2} \left(\frac{2m_r}{\hbar^2}\right)^{3/2} \sqrt{\hbar\omega - E_{\Gamma,(HH,LH)}}$  are the

joint density of states for the  $\Gamma$  and HH bands and the  $\Gamma$  and LH bands with  $m_r$  the reduced

effective mass defined by  $\frac{1}{m_r} = \frac{1}{m_{\Gamma}} + \frac{1}{m_{LH,HH}}$ . We use the following effective mass of density

of states:  $m_{HH} = 0.284m_0$  ( $m_{LH} = 0.043m_0$ )<sup>[4]</sup>  $m_{\Gamma} = 0.038m_0$  ( $m_L = 0.56m_0$ ).<sup>[5]</sup> Note

that this formula supposes dipolar interactions between stationary conduction band and

valence band states assuming a homogeneous broadening of zero for each transition. In reality

the carrier interactions with vibrational modes of the crystal (phonon) and scattering effects

lead to a homogeneous broadening that can be accounted for by introducing a Lorentzian

shape to the transition by using the following equation:<sup>[3]</sup>

$$\alpha_{TE, TM}^{HH, LH}(\hbar\omega) = C_0 |D_{HH, LH}^{TE, TM}|^2 \int_0^{\infty} dE \rho_{HH, LH}(E) \times [f_c(E) - f_v(E)] \frac{\Gamma_0/2\pi}{(\Gamma_0/2)^2 + (E_{\Gamma,(HH,LH)} + E - \hbar\omega)^2}$$

(S3)

where  $\Gamma_0$  is the full width at half maximum (FWHM) energy of the transition. We assume that

$D_{HH, LH}^{TE, TM}$  is independent from  $\mathbf{k}$ .<sup>[3]</sup> Note that this spectral broadening introduced in the model

induces a decrease of the gain amplitude since the Lorentzian function is normalized to unity

due to the conservation of the transition oscillator strength.

Fermi statistics  $f_c(E)$  for electrons and  $f_v(E)$  for holes allow one to calculate the carrier

spatial distribution taking into account the band edge energy spatial variation induced by

strain. One can suppose that strain in the range of 1-2% will not produce significant changes of the doping across the layer so that the electron density  $N_d$  introduced by the doping is considered as constant across the Ge layer. Note that the electron distribution is weakly dependent on the position of the  $\Gamma$  valley which exhibits a low density of states due to the low effective mass  $m_\Gamma = 0.038m_0$  as compared to the L valley  $m_L = 0.56m_0$ . The excess carrier density distribution introduced by an external optical pumping of the germanium,  $n$  and  $p$ , are computed such that the carrier density at the  $z$ -position corresponding to the lower band energy point (in general near the top surface) is fixed at a chosen value. Different values can be estimated independently considering the generation recombination balance equation for a given optical pumping power density and by using proper relaxation rates depending on the experimental conditions and on the material properties.

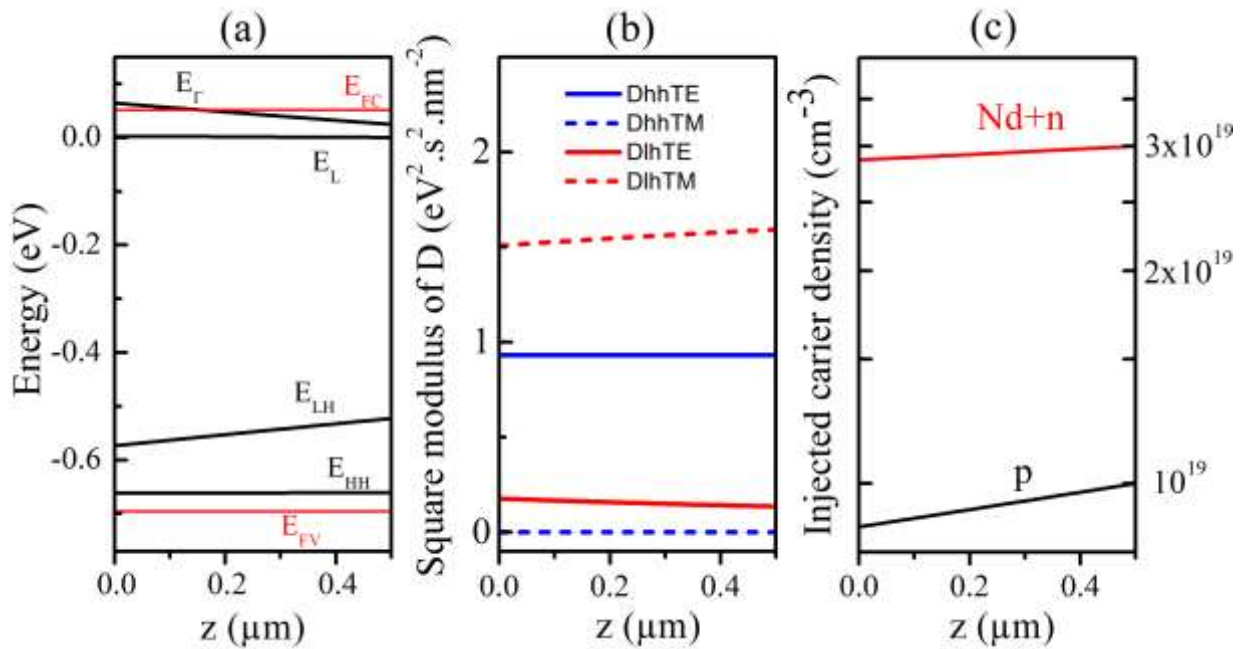


**Figure S2.** (a) Conduction and valence band energies across the Ge layer (b) Square modulus of dipolar matrix elements profile for TE and TM polarizations and for both direct  $\Gamma$  -LH and  $\Gamma$ -HH transitions (c) Carrier density profiles across the Ge layer.

The quasi-Fermi level is then pinned at the corresponding energy and is considered as constant for the rest of all the positions across the layer. The carrier density inside the layer is

then calculated with this fixed value of the Fermi level. The valence band energy variation across the layer induces a variation of the carrier densities. Note that the total electron density is such that  $N = N_d + n$  with  $n = p$ . These carrier density distributions are then introduced to calculate the free-carrier absorption (FCA) profile across the layer. The parameters for the wavelength dependent free-carrier absorption are taken from Ref. [6]. Figure S2c shows the carrier density distribution across the Ge layer. As can be seen, the hole density was fixed to  $10^{19} \text{cm}^{-3}$  near the surface and the band bending due to strain variation induces a variation of the hole density across the layer. In this example a doping density of  $2 \times 10^{19} \text{cm}^{-3}$  was considered.

The total net gain profile is calculated by summing the results from equation S2 (or S3 if considering a homogeneous broadening) and the FCA profile (calculated using the total carrier density profiles) at each z-position. This leads to the net gain profile at 1900 nm wavelength as the one presented in Figure 3a for TM polarization. The optical field distribution  $E(z)$  of the confined mode in the layer is calculated for TM (TE) polarization and then introduced in a final integration with the net gain profile to calculate the total modal gain in the structure. This process is realized at each wavelength of the gain spectrum. The field distribution is evaluated at several wavelengths to account for modal dispersion of the guided light in the layer. The net modal gain spectrum is then calculated for various excess carrier densities and level of doping as reported in **Figure S3**. The maximum gain of the spectrum as obtained from Figure S3 is then reported in the Figure 3c. The electromagnetic field distribution accounts for the vertical confinement only. This approximation provides a satisfactory description since the strain and the gain are quasi constant in the layer plane.

Submitted to

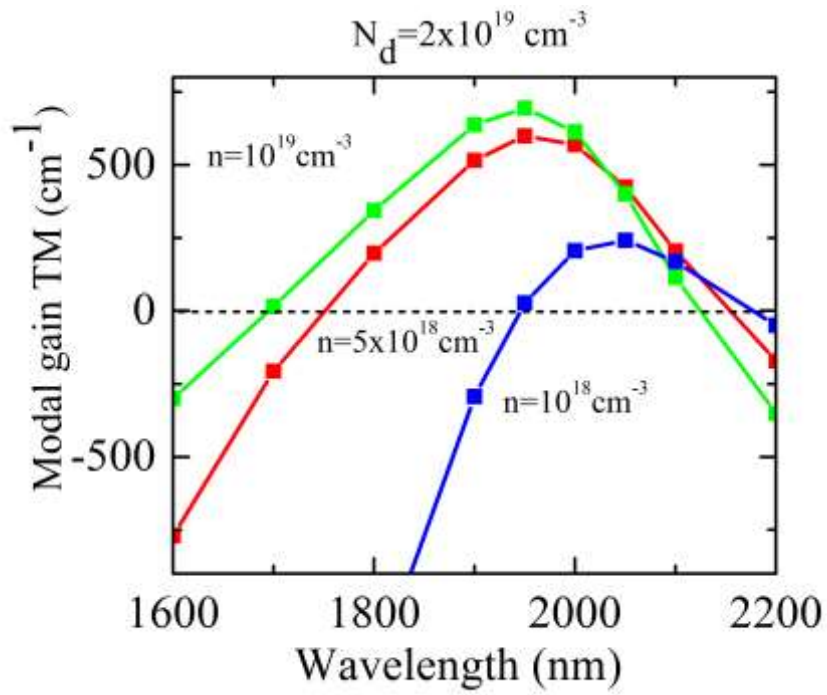


**Figure S3.** Modal gain spectra for different excess carrier densities assuming a  $2 \times 10^{19} \text{ cm}^{-3}$  doping density calculated using equation S2.

**Microdisk emission under high injection level**

*Abdelhamid Ghrib,\* Moustafa El Kurdi,\* Mathias Prost, Sébastien Sauvage, Xavier Checoury, Grégoire Beaudoin, Marc Chaigneau, Razvigor Ossikovski, Isabelle Sagnes, Philippe Boucaud*

We have performed pulsed pumping experiments on the all-around stressed microdisk at high power in order to reach sufficient carrier injection for gain achievement (**Figure S4**). The pulse duration of the pumping laser at 930 nm wavelength is 4 ns and the repetition period is 40  $\mu$ s. The maximum peak power is varied from 0.6 W to 6 W, and the beam is focused into a 10  $\mu$ m spot diameter on the sample surface. These pumping conditions allow one to realize a high level of pumping while avoiding heating effects as can be observed for cw pumping of suspended membranes.<sup>[7,8]</sup> At the lower level of pumping power, the spectrum is similar to the one observed for low pumping power in cw with a maximum of the emission around 2  $\mu$ m wavelength and is dominated by the fundamental direct band gap transition involving recombination with light holes  $\Gamma$ -LH (Figure 2d). Note that the signal is analysed with an extended InGaAs photodiode cooled at -85° C which exhibits a cut-off wavelength at 2050 nm, while for the measurements of Figure 2d the photodiode was used at room temperature to reach larger cut-off wavelength. When the power is increased from 0.6 W to 6 W the emission is blue shifted so that the contribution from  $\Gamma$ -HH becomes dominant on the spectrum as shown in Figure S4a. This spectral dependence with power is well reproduced in the modelling of the emission when the excess carrier density is increased from  $2 \times 10^{18} \text{ cm}^{-3}$  to  $1.6 \times 10^{19} \text{ cm}^{-3}$  (see Figure S4b). It explains why we indicate in the text that we can obtain a photo-induced carrier density in the  $10^{19} \text{ cm}^{-3}$  range.

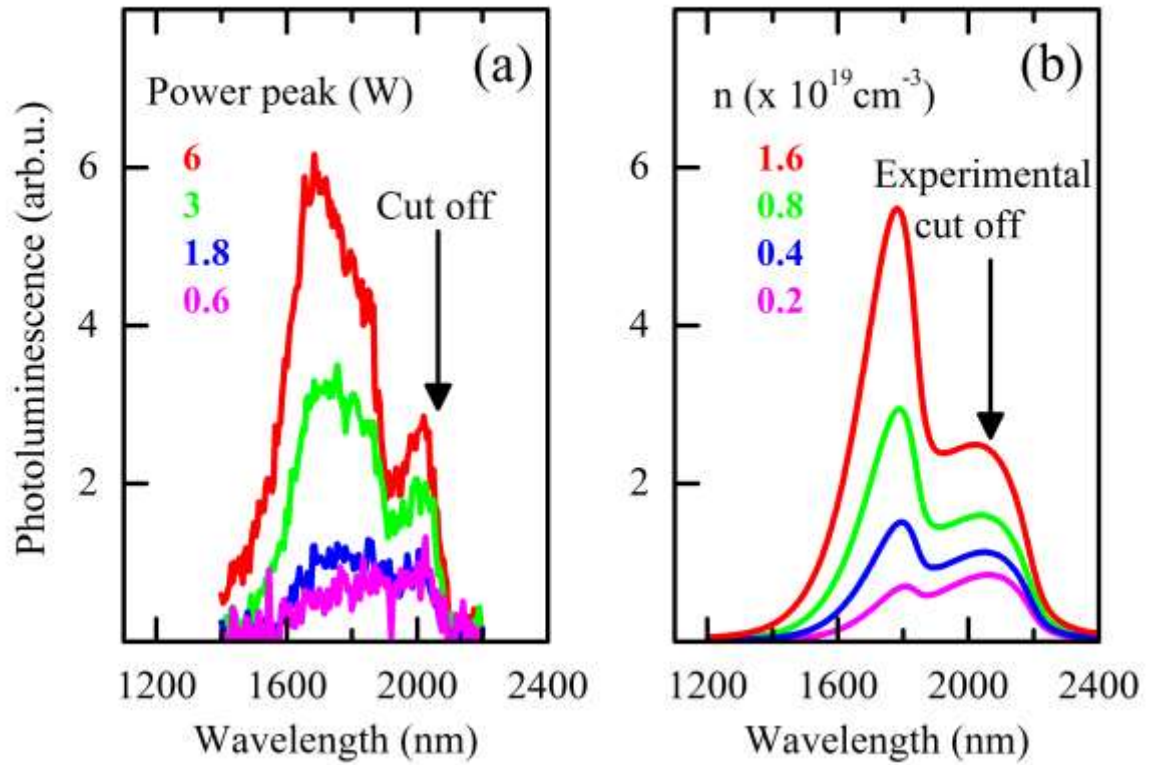


**Figure S4.** (a) Experimental photoluminescence spectrum of the all-around stressed microdisk under pulsed pumping for different pump powers (b) calculated spectrum for various injected carrier densities in order to reproduce the experimental spectrum dependence as a function of the increasing power.

Submitted to

- [1] A. Ghrib, M. El Kurdi, M. de Kersauson, M. Prost, S. Sauvage, X. Checoury, G. Beaudoin, I. Sagnes, P. Boucaud, *Appl. Phys. Lett.* **2013**, *102*, 221112.
- [2] M. El Kurdi, G. Fishman, S. Sauvage, P. Boucaud, *J. Appl. Phys.* **2010**, *107*, 013710.
- [3] S. L. Chuang, *Physics of Optoelectronic Devices*, Wiley, New York, **1995**.
- [4] R. N. Dexter, H. J. Zeiger, B. Lax, *Phys. Rev.* **1956**, *104*, 637.
- [5] D. Bimberg, O. Madelung, *Physics of Group IV Elements and III-V Compounds*, Springer, Berlin, **1982**.
- [6] P. Boucaud, M. El Kurdi, A. Ghrib, M. Prost, M. de Kersauson, S. Sauvage, F. Aniel, X. Checoury, G. Beaudoin, L. Largeau, I. Sagnes, G. Ndong, M. Chaigneau, R. Ossikovski, *Photonics Res.* **2013**, *1*, 102.
- [7] G. Shambat, S. Cheng, J. Lu, Y. Nishi, J. Vuckovic, *Appl. Phys. Lett.* **2010**, *97*, 241102.
- [8] P. Boucaud, M. El Kurdi, S. Sauvage, M. De Kersauson, A. Ghrib, X. Checoury, *Nat. Photonics* **2013**, *7*, 162.